Supplemental Material of Effects of Hydrogen Transport on the Kinetic Regimes of 4-Nitrophenol Reduction by Sodium Borohydride

Tatiana Nizkaia, Philipp Groppe, Valentin Müller, Jens Harting, Susanne Wintzheimer, and Paolo Malgaretti

ASSUMPTIONS AND APPROXIMATIONS OF THE MODEL

In order to minimize the number of parameters, we used the following simplifications in deriving the model, described in Eqs.(4a-4c) of the main text.

First, we use an effective pseudo zeroth-order reaction scheme for H_2 mediated hydrogenation of 4-NiP at all times. The effective pseudo zeroth order kinetics observed in the experiments [1, 2] supposedly follows from the microscopic binding-unbinding kinetics of 4-NiP to the Pt nanoparticles and the reaction of the adsorbed species with dissolved hydrogen (Eley-Rideal mechanism [3]):

$$\frac{dC_{\text{4-NiP}}}{dt} = k_A \theta_{\text{4-NiP}} C_{H_2}, \tag{S1}$$

where k_A is proportional to the available surface of the catalyst and $\theta_{\text{4-NiP}}$ is the fraction of the catalyst occupied with 4-NiP:

$$\theta_{\text{4-NiP}} = \frac{K_{\text{4-NiP}} C_{\text{4-NiP}}}{1 + K_{\text{4-NiP}} C_{\text{4-NiP}}}, \tag{S2}$$

where $K_{\text{4-NiP}}$ is the adsorption equilibrium constant of 4-NiP. When $K_{\text{4-NiP}} C_{\text{4-NiP}} \gg 1$, $\theta_{\text{4-NiP}} \approx 1$ and the kinetics is pseudo zero-the order in 4-NiP. This behavior is expected to break at small densities of 4-NiP, where the full equation for coverage has to be taken into account.

Second, we do not explicitly use Langmuir-Hinshelwood model [4] (accounting for the competition of the reactants for the active sites at the catalysts) to describe the surface reaction between borohydride and 4-NiP. In the literature [5–7] Langmuir-Hinshelwood approach is used to fit the dependence of the short term apparent reaction rate k_{app} on initial concentrations. We use instead a simple binary reaction term with an *effective* rate coefficient k_{AB}, which can also depend on the initial concentrations of the reactants.

Third, we have disregarded all back-reactions, since our focus is mainly on the intermediate stages of the time evolution of the 4-NiP concentration, rather than on the eventual equilibrium state or on the initial short term effects. In particular, we disregard here the induction period, associated with the back-reaction of 4-aminophenol with dissolved oxygen [8–11], because in our experiments this induction period was shorter than the time resolution of measurements. This back reaction might also be important at late stages of the reduction process and at large surface to volume ratios, when dissolved oxygen, adsorbed from the atmosphere, starts to dominate over hydrogen.

Finally, we adopt a linear dependence of the hydrogen evaporation flux on the dissolved hydrogen concentration $C_{\mathrm{H_2}}$, neglecting the saturation concentration of H_2. This approximation is justified for evaporation from an open, stirred beaker into the atmosphere, since hydrogen is much lighter than air and does not accumulate near the gas-liquid interface. However, when an oversaturated solution is in direct contact with growing hydrogen bubbles, the effective saturation concentration depends on the bubble size through the Laplace pressure, breaking the linear dependence of te flux on C_{H_2}. Consequently, while the coefficient α_l corresponds to the degassing rate from a stirred beaker and can be estimated using gas-liquid mass-transfer models [12], the coefficient α_s should be regarded as an empirical parameter.

DATA FITTING PROCEDURE

We fit the data presented in using the theoretical model. Not surprisingly, having 4 fitting parameters for each experimental curve allows us to fit all the experimental data with high accuracy. However, is it to be expected that upon changing the concentration of $CaCl_2$ *all* the rate constants have to change?

First, we can expect that the hydrogen transport rate α in the non-bubbling regime should be the same for all supraparticles, because it is associated with the rate of H_2 evaporation from the reactor. Indeed, we can extract α by fitting the experimental data for $t > 7$ min. For both types of particles an excellent fit is obtained with $\alpha = 0.075$ min^{-1}. Second, the collapse of the experimental data for $t > 7$ min (see Fig. 4b in the main text) implies that both the hydrolysis of borohydride and the hydrogenation of 4-NiP via dissolved H_2 occur

at very similar rates for the particles of this set i.e. k_A and k_B should be the same for all Type A supraparticles.

Interestingly, it is indeed possible to fit all the data for particles of Type A and Type B with the same values of k_A, k_B, α_s, α_l and t_{bub} taken from the experiment, by solely varying k_{AB}. We use the following set of common parameters:

$$k_B = 0.0075\, s^{-1}, k_A = 1.45 \cdot 10^{-7}\, s^{-1},$$
$$\alpha_l = 1.25 \cdot 10^{-3}\, s^{-1}, \alpha_s = 4.8 \cdot 10^{-3}\, s^{-1}, \tag{S3}$$

and the following values of bubbling time, based on experimental observations:

$$\text{Type A: } t_{bub} = 7\,\text{min}, \tag{S4}$$
$$\text{Type B (non-bubbling): } t_{bub} = 0\,\text{min}. \tag{S5}$$

The values of k_{AB} are fitted for each curve individually.

We remark, however, that the set of fitting parameters chosen above is not unique. Indeed, while the long-term collapse of the reaction rate curves for Type A particles imposes clear restrictions on the reaction rate coefficients, the data for supraparticles of Type B is compatible with different scenarios. As shown in the top panels of Fig. S1, the same data can be fitted successfully using different assumptions. For example, the fit shown in Fig. S1a accounts for both chemical pathways at the same time and uses the same values k_A, k_B, α as for Type A particles and varying k_{AB}. The fit in Fig.S1b accounts only for transfer hydrogenation of 4-NiP by $NaBH_4$ with $k_A = 0$, the same values of k_B for all curves and varying k_{AB}. Finally, Fig. S1c shows a fit assuming only H_2-mediated hydrogenation of 4-NiP, with $k_{AB} = 0$ and varying k_A, k_B, α. Therefore, in this case it is not possible to identify the relative importance of the two chemical pathways by studying only the evolution of 4-NiP concentration. However, while the resulting $c_{\text{4-NiP}}$ curves are very similar, the time evolution of the H_2 concentration in the solution is different, as shown in the corresponding bottom panels in Fig. S1. The bottom panels of Fig. S1 show that the full model accounting for both chemical pathways leads to a time evolution of the H_2 concentration on a time scale,

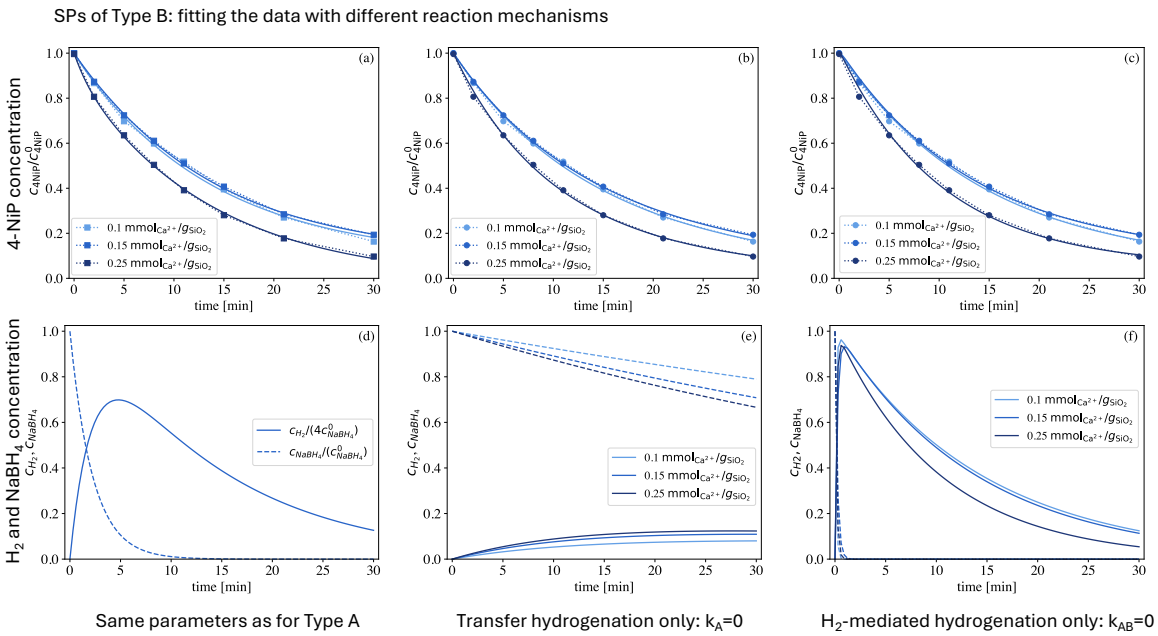

FIG. S1. 4-NiP concentration (top) and modeled H_2 concentration (bottom) for particles with 19 nm SiO_2 grains, fabricated with different concentrations of $CaCl_2$. Solid lines are fits using Eqs. (**??-??**) with the following sets of parameters: (a,d) k_A, k_B, α defined by Eq.(S3) and varying k_{AB} (same parameters as for 182 nm) (b,e) $k_A = 0$, $\alpha = 1.25 \cdot 10^{-3}\, s^{-1}$ and k_{AB}, k_B fitted for each curve (hydrogenation only by surface reaction with borohydride), (c,f) $k_{AB} = 0$ and fitted k_A, k_B, α (hydrogenation only by dissolved H_2).

similar to what was observed for the H_2 flux in experiments on concurrent hydrolysis and 4-NiP hydrogenation (see Fig. 1b in [13]). At variance, accounting for solely one of the two chemical pathways leads to either monotonic growth of the concentration of H_2 (Fig.S1e)[14], or a very steep surge of H_2 concentration (Fig.S1f), followed by slow relaxation.

Therefore, our model suggests a route to identify the underlying chemical pathway by performing simple additional measurements. In fact, since in our model the outflow of hydrogen is proportional to its concentration, measuring of H_2 flux in the experimental condition may differentiate between the different reaction mechanisms. Note, that the measurements of hydrogen flux do not need to be very precise: it is sufficient to estimate whether the flux increases, decreases or experiences a non-monotonous evolution in time.

While different sets of parameters may be used to fit the experimental curves with the model in Eqs. (**??**), we find the one proposed in Eq.(S3) particularly interesting since it allows us to fit all experimental curves upon varying a single parameter k_{AB}.

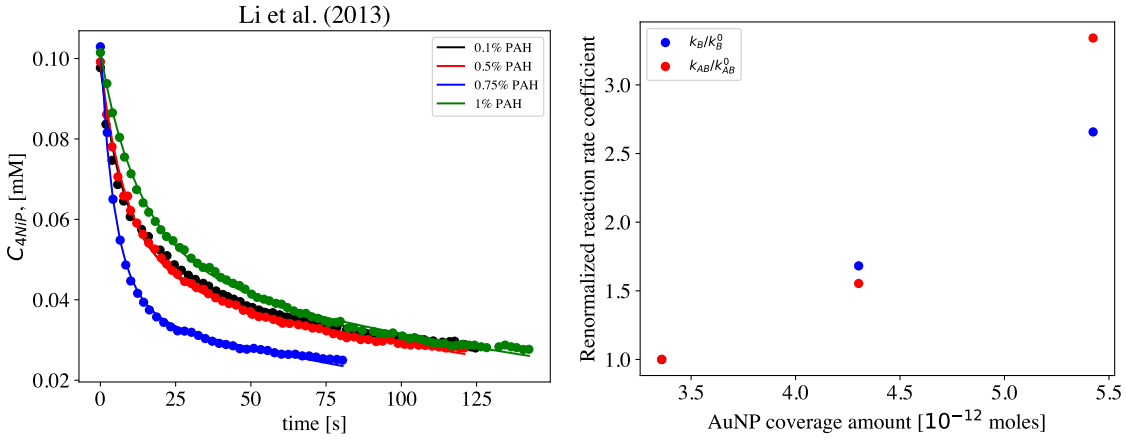

FIG. S2. 4-NiP concentration (left) and fitted reaction rates (right) for 4-NiP reduction on Au-NP embedded onto polymeric spheres. Data taken from [16] is represented by circles, solid curves are fits using our model Eq.(4a-4c).

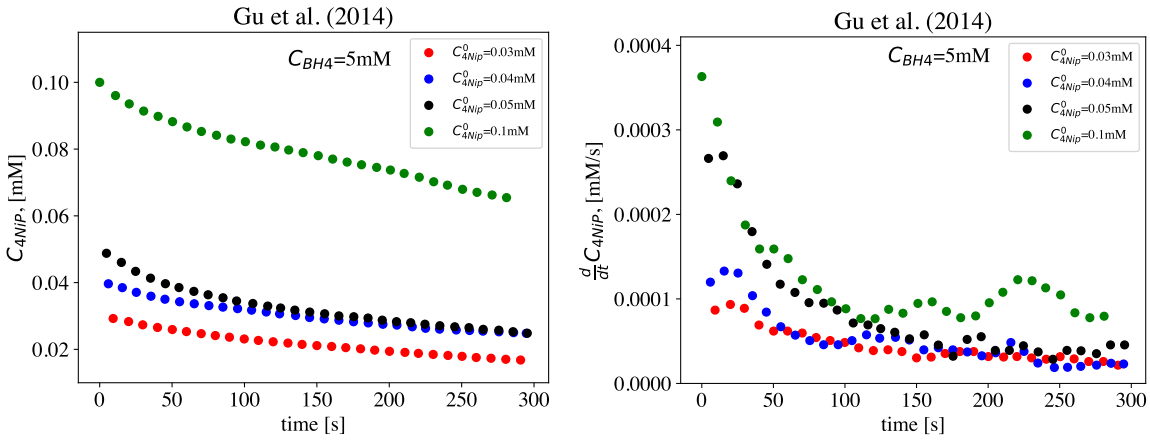

FIG. S3. 4-NiP concentration (left) and its time derivative (right) for different initial concentrations of 4-NiP. Data taken from Ref.[17], Fig.3.

ANALYSIS OF LITERATURE DATA

In this section we revisit previously published data on 4-nitrophenol reduction, focusing on the studies where deviations from pseudo-first-order kinetics have been reported. The datasets have been extracted from the figures of corresponding papers using the online tool Automeris v5 [15].

We start by revisiting work by Li et al.[16], in which Au nanoparticles supported by polymeric sub-microspheres were used as the catalyst. In this work authors observed significant deviations of 4-NiP reduction kinetics from pseudo-first order and reported formation of H_2

bubbles. To explain the data the authors proposed a fractional order kinetic model with respect to 4-NiP and found that the reaction order depends on the surface coverage of Au particles. However, we note that the apparent fractional order kinetics can also result from an overlap of two different kinetic regimes operating at similar time scales. To illustrate the point, we took the concentration curves from Fig.3 in [16] and fitted them using our two-mechanisms model Eq.(4a-4c)(solid curves in Fig. S2a). We can see that the apparent fractional order arises naturally when both hydrolysis and hydrogenation rates increase with increasing Au-NP coverage (see fitted parameters k_B, k_{AB} provided in Fig.S2b). Interestingly, a similar system with silver nanoparticles on a resin support [18] did not show any deviations from pseudo first order kinetics despite the reported presence of H_2 bubbles. This is in line with the fact that Ag nanoparticles do not catalyse H_2-mediated hydrgogenation, because dissociative adsorprion of hydrogen on silver is very weak [13]. Therefore only mechanism I (binary reaction between 4-NiP and $NaBH_4$ on the surface of the catalyst) with first-order reaction kinetics is present.

Kinetics with different apparent reaction rates at short and long times has been also observed and studied in [6, 17]. To explain this behavior authors proposed a reaction scheme involving formation of an intermediate species (4-hydroxylaminophenol) that has a very strong adsorption to Pt and blocks the active sites causing the slowdown of the reaction. Our model provides an simple alternative explanation to this behavior: a shift from direct reaction with borohydride to hydrogenation via dissolved H_2. To illustrate our point, we have extracted the data from Fig.3 in [17], featuring 4-NiP reduction by $NaBH_4$ on SPB $-$ $Au_{75}Pd_{25}$ nanoalloys at different initial concentrations of 4-NiP and $NaBH_4$. While the plots in [17] are provided in terms of the ratio $C_{\text{4-NiP}}/C^0_{\text{4-NiP}}$, we reconstruct the 4-NiP concentration and reduction rate curves, by multiplying the data by the respective initial concentration $C^0_{\text{4-NiP}}$ (see Fig.S3). Interestingly, at large excess of borohydride $C^0_{\text{NaBH}_4}/C^0_{\text{4-NiP}} > 100$ (red, blue and black symbols in Fig.S3) we observe the collapse of the reaction rate curves at long times, similar to what we have witnessed for Type A particles. Such collapse is typical for the transition from borhydride-mediated to H_2-mediated reduction of 4-NiP. Moreover, the non-monotonous shape of the rate curve for $C^0_{\text{4-NiP}} = 0.1\ mM$ suggests a reaction acceleration associated with transition from bubbling to non-bubbling regime and build-up of dissolved H_2, similar to what was observed for Type C particles. However, since the presence or absence of bubbling

has not been reported in [17], it is impossible to check this hypothesis.

[1] M. J. Vaidya, S. M. Kulkarni, and R. V. Chaudhari, Synthesis of p-aminophenol by catalytic hydrogenation of p-nitrophenol, Organic Process Research & Development **7**, 202 (2003).

[2] R. Grzeschik, D. Schäfer, T. Holtum, S. Küpper, A. Hoffmann, and S. Schlücker, On the overlooked critical role of the ph value on the kinetics of the 4-nitrophenol nabh4-reduction catalyzed by noble-metal nanoparticles (pt, pd, and au), The Journal of Physical Chemistry C **124**, 2939 (2020).

[3] D. D. Eley and E. K. Rideal, The heterogeneous catalysis of the decomposition of hydrogen peroxide, Proceedings of the Royal Society of London. Series A, Mathematical and Physical Sciences **178**, 429 (1938).

[4] I. Langmuir and C. N. Hinshelwood, The mechanism of homogeneous hydrogenation, Transactions of the Faraday Society **24**, 662 (1928).

[5] S. Wunder, F. Polzer, Y. Lu, Y. Mei, and M. Ballauff, Kinetic analysis of catalytic reduction of 4-nitrophenol by metallic nanoparticles immobilized in spherical polyelectrolyte brushes, The Journal of Physical Chemistry C **114**, 8814 (2010).

[6] S. Gu, S. Wunder, Y. Lu, M. Ballauff, R. Fenger, K. Rademann, B. Jaquet, and A. Zaccone, Kinetic analysis of the catalytic reduction of 4-nitrophenol by metallic nanoparticles, The Journal of Physical Chemistry C **118**, 18618 (2014).

[7] A. Iben Ayad, D. Luart, A. Ould Dris, and E. Guénin, Kinetic analysis of 4-nitrophenol reduction by "water-soluble" palladium nanoparticles, Nanomaterials **10**, 1169 (2020).

[8] Z. Wu, J. Zhu, W. Wen, X. Zhang, and S. Wang, Spherical covalent organic framework supported cu/ag bimetallic nanoparticles with highly catalytic activity for reduction of 4-nitrophenol, Journal of Solid State Chemistry **311**, 123116 (2022).

[9] E. Menumerov, R. A. Hughes, and S. Neretina, Catalytic reduction of 4-nitrophenol: a quantitative assessment of the role of dissolved oxygen in determining the induction time, Nano letters **16**, 7791 (2016).

[10] J. Strachan, C. Barnett, A. F. Masters, and T. Maschmeyer, 4-nitrophenol reduction: probing the putative mechanism of the model reaction, ACS Catalysis **10**, 5516 (2020).

[11] R. D. Neal, E. Menumerov, R. A. Hughes, and S. Neretina, Catalytic reduction of 4-nitrophenol by gold catalysts: The influence of borohydride concentration on the induction time, The Journal of Physical Chemistry C **123**, 18702 (2019).

[12] P. V. Danckwerts *et al.*, *Gas-liquid reactions* (McGraw-Hill New York, 1970).

[13] S. Varshney, D. Meyerstein, R. Bar-Ziv, and T. Zidki, The competition between 4-nitrophenol reduction and bh4- hydrolysis on metal nanoparticle catalysts, Molecules **28**, 6530 (2023).

[14] We remark that the fit in Fig.S1b does not fix the value of α. Hence, in order to estimate the time evolution of H_2 in Fig.S1e we used the same value of k_α that we used for Type A supraparticles and Fig.S1a.

[15] Automeris: Web-based plot digitizer, `https://automeris.io`, online tool for data extraction from images, accessed: 2026-01-21.

[16] M. Li and G. Chen, Revisiting catalytic model reaction p-nitrophenol/nabh 4 using metallic nanoparticles coated on polymeric spheres, Nanoscale **5**, 11919 (2013).

[17] S. Gu, Y. Lu, J. Kaiser, M. Albrecht, and M. Ballauff, Kinetic analysis of the reduction of 4-nitrophenol catalyzed by au/pd nanoalloys immobilized in spherical polyelectrolyte brushes, Physical Chemistry Chemical Physics **17**, 28137 (2015).

[18] T. Kanti Das, S. Ganguly, S. Remanan, and N. C. Das, Temperature-dependent study of catalytic ag nanoparticles entrapped resin nanocomposite towards reduction of 4-nitrophenol, ChemistrySelect **4**, 3665 (2019).